J Mater Sci (2008) 43:6391–6399
DOI 10.1007/s10853-008-2687-x

Spark Plasma synthesis and diffusion of Cu and Ag in vanadium mixed valence oxides

Jean Galy · J. Ph. Monchoux

Received: 29 November 2007 / Accepted: 29 April 2008 / Published online: 9 July 2008

Abstract Spark Plasma sintering (SPS) technique allows powders to be compacted at low temperature with a very short holding time. The powder loaded into a carbon die is heated via direct current pulses and simultaneously submitted to an uni-axial pressure of several MPa. Full density of the sample is achieved within minutes. This process is used to study Cu and Ag metals interactions with V_2O_5 oxide. Syntheses of $M_xV_2O_5$ phases (M = Cu, Ag) have been achieved within minutes. Thus Cu and Ag atoms penetrate microcrystals of V_2O_5 oxide at a high speed, shearing its crystal network and simultaneously rebuilding the crystal structures of the prototype networks β, β', ε or δ $M_xV_2O_5$. To account for the formation of these phases identified by X-ray diffraction, structural mechanisms are proposed. Cu and Ag atomic diffusion parameters have been determined from energy dispersive X-ray spectroscopy (EDX) and electron micropobe analysis (EPMA) line scans. High values of diffusion coefficients have been determined. Cu atoms diffuse faster than Ag, $D_{Cu} \approx 4 \times 10^{-8}$ m^2/s and $D_{Ag} \approx 0.5$–1×10^{-9} m^2/s in ε and δ $M_xV_2O_5$ phases, respectively. Their formation may also be used as a model for further investigations into the diffusion mechanisms of atoms in solids and for a better understanding of the SPS process.

J. Galy (✉) · J. Ph. Monchoux
Centre d'Elaboration de Matériaux et d'Etudes Structurales-CNRS, 29, rue Jeanne Marvig, BP 94347, 31055 Toulouse Cedex 4, France
e-mail: galy@cemes.fr

Introduction

Spark Plasma sintering (SPS) is an unconventional technique for sintering materials which offers undeniable advantages in terms of quality and efficiency. Several papers confirm its widespread use and investigate the influence of a number of parameters [1–6]. The SP technique has already been used as a synthesis tool in few systems as for examples $MoSi_2$ [6], superconductor MgB_2 [7] and some others [8–11] The general protocol for SPS experiments consists in inserting the powder into a graphite die, two punches closing the unit. The powder is in contact through graphite and stainless steel spacers with the electrodes. The uni-axial pressure is supported by the latter device. The die and its sample are subjected to DC electric current pulses. Heat transfer is easy, the graphite die also acting as a heating element.

Among the wide range of vanadium oxide bronzes established for the first time for sodium and lithium by Wadsley [12, 13], the M–V–O systems (M = Cu and Ag) exhibit several phases $Cu_xV_2O_5$ (α, β', ε) and $Cu_xV_4O_{11}$, and $Ag_xV_2O_5$ (α, β, δ) whose homogeneity ranges, crystal structures and physical or electrochemical properties have been studied [14–20]. In these bronzes marked by the nonstoichiometry in Cu and Ag and the mixed valence of vanadium (V^{5+} and V^{4+}), one salient feature is also the mixed valence of copper (Cu^+ and Cu^{2+}).

To assess the potential of the Spark Plasma technique, not only in terms of powder sintering, but also as a synthesis process, M–V–O systems have been investigated. A preliminary experiment was conducted using copper and vanadium pentoxide powders. V_2O_5 exhibits a layered structure in which layers are built up by VO_5 square pyramids sharing edges and corners (Fig. 1) [21].

A sandwich of V_2O_5–Cu–V_2O_5 powders was prepared in a carbon die and placed in the Sumitomo 2080 Spark

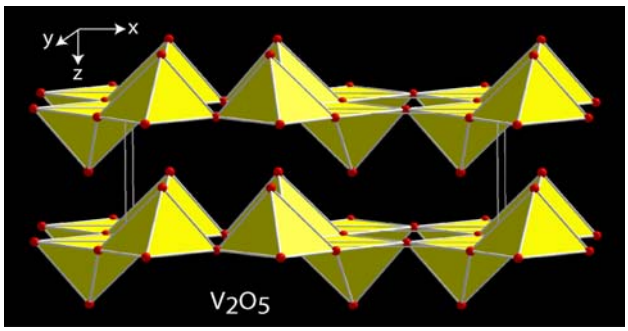

Fig. 1 The layer structure of V_2O_5 built up with VO_5 square pyramids

Plasma machine operating in the "Plate-forme Nationale de Frittage Flash/CNRS" in Toulouse.[1] For each pellet, a weighed amount of powder was placed in an 8-mm inner diameter carbon die to achieve a dense 3-mm thick V_2O_5 and 2-mm thick Cu unique compact. Under a fixed uniaxial pressure of 50 MPa, the pellet was first heated via DC electric pulses of 3.3 ms from 20 to 600 °C in 6 min and then subjected to rapid quenching. Compaction of pellets was above 95%. The cross section of the pellet revealed a surprising ultra fast reaction highlighted by the appearance of a blue–black phase, which given its colour, could be a reduced vanadium oxide V_2O_{5-x} or a $Cu_xV_2O_5$ bronze. The blue zone can be seen between the red Cu layer and the yellow-orange V_2O_5 layer (Fig. 2).

An electron probe analysis performed perpendicularly to the successive layers clearly shows that copper atoms have migrated and created the blue phase, a $Cu_xV_2O_5$ bronze (Fig. 3). This blue phase extends symmetrically on either side of Cu slab and with a slow decrease in copper concentrations as indicated by the smooth slopes of their linear regression analyses.

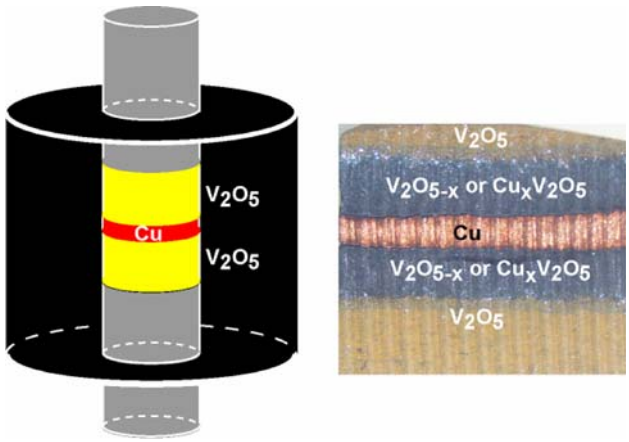

Fig. 2 Schematic view of the graphite die containing its successive layers of V_2O_5 and Cu powders (*left*) and pellet cross section after Spark Plasma treatment (*right*)

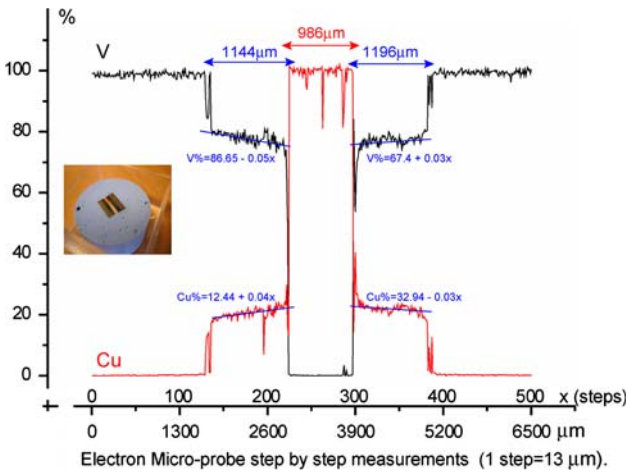

Fig. 3 Electron microprobe analysis performed on the cross section perpendicular to the Cu slab

Experimental

Starting powders

Vanadium pentoxide (99.6+%), Copper (99.5%) (Aldrich) and silver (99.9%) (Alfa Aesar) powders were used in these experiments.

SPS process

Spark Plasma experiments have been conducted using Dr. Sinter 2080 Syntex machine, which allows temperatures up to 2000 °C via sequences of 12 pulses of 3.2 ms of current followed by two pulses without (maximum amperes 8000 A) and pressures up to 200 MPa. The machine belongs to PNF2/CNRS.

Powders were inserted into a die, then closed by two punches; these elements being made of graphite 2333 grade from Carbone Lorraine.

XRD

XRPD patterns were recorded at room temperature in the 2θ range 5° to 55° (2θ) in steps of 0.02° and counting rates of 10 s, with a SEIFERT XRD 3000 diffractometer using a graphite monochromatized Cu$K\alpha$ radiation. Unit cell parameters were derived from these data after *hkl* indexing of all diffraction peaks and least square refinement using the CELREF program.

[1] PNF2/CNRS, Module Haute Technologie, Université Paul Sabatier, Toulouse, France. Established by P. Millet, P. Rozier & J. Galy, CEMES-CNRS, 2003–2004.

Analyses

Analyses of SPS pellets cross sections were performed with a microprobe CAMECA SX 50 (Samx automation) at the "Service Microsonde Electronique" (Laboratoire des Mécanismes et Transferts en Géologie—LMTG—Toulouse University, France). Analytical conditions were 15 kV, 20 nA, 10 s counting time on peak and 5 s for background. Standards used were Cu or Ag metals and V_2O_5.

Other pellets have been metallographically prepared (grinding by SiC papers and polishing by diamond pastes down to 3 μm). Growth of $M_xV_2O_5$ phases was followed by back-scattered electron (BSE) imaging and energy dispersive spectrometry (EDS) line-scans in a Jeol JSM 6700 F scanning electron microscope (SEM). The EDS signal was calibrated on standards of known Cu and Ag concentrations.

Crystal chemistry of $M_xV_2O_5$ bronzes

Polycrystalline samples of $Cu_xV_2O_5$ and $Ag_xV_2O_5$ phases have been prepared by solid state reaction of Cu, Ag and V_2O_5 powders mixed in an agate mortar, sealed in quartz tubes and reacted at 600 °C during two 24 h runs separated by grinding. All samples showing a blue–black colour were carefully controlled by X-ray powder diffraction (XRPD). All the structures pertaining to these phases were determined on single crystals obtained by melting and slow cooling.

For $0 < x < 1$ these bronzes exhibit three different phases:

- an α phase for $0 < x < 0.02$ with intercalation of a few Cu or Ag atoms between the $[V_2O_5]_n$ layers of the vanadium pentoxide structure;
- a β' and β phase with $0.26 < x < 0.64$ for Cu and $0.29 < x < 0.41$ for Ag whose structures [15, 20] are derived from the Wadsley's β $Na_xV_2O_5$ tunnel network [12]. These phases exhibit a $[V_2O_5]_n$ three-dimensional network M metal atoms being inserted into oxygenated tunnels running along [010], the shortest b parameter

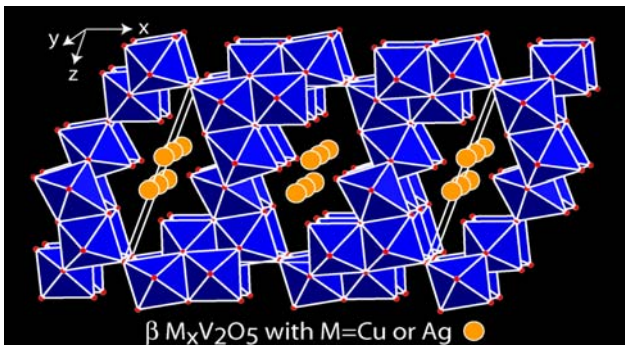

Fig. 4 Perspective view of the β or β' structure types

(Fig. 4). They crystallize in the monoclinic system—with, for Cu, space group *Cm* and $a = 15.2007$Å, $b = 3.6375$Å, $c = 10.0925$Å, $\beta = 106.13$ for $x = 0.59$ [17] and, for Ag, space group *C2/m* and $a = 15.388$ Å, $b = 3.6139$ Å, $c = 10.088$ Å, $\beta = 109.94°$ for $x = 0.40$ [20].

For higher concentration in M, two layered structure types are formed with $[V_2O_5]_n$ double layers, both crystallizing in the monoclinic system, $-\varepsilon Cu_xV_2O_5$ with $0.85 < x < 1$, space group Cm and $a = 11.780$ Å, $b = 3.691$ Å, $c = 8.876$ Å, $\beta = 111.8$ for $x = 0.85$ [15] and, for Ag with $0.68 < x < 0.81$, space group *C2/m* and $a = 11.742$ Å, $b = 3.667$ Å, $c = 8.738$ Å, $\beta = 90.48$ for $x = 0.68$ [19]. A perspective view of these two structures is given in Fig. 5.

The structural relationship between these various structures and the original network of V_2O_5 has been described elsewhere [22].

Experiments—interpretation

$Cu–V_2O_5$ case

Given the unexpected ultra fast reaction of Cu with V_2O_5, new experiments were conducted by varying reaction time.

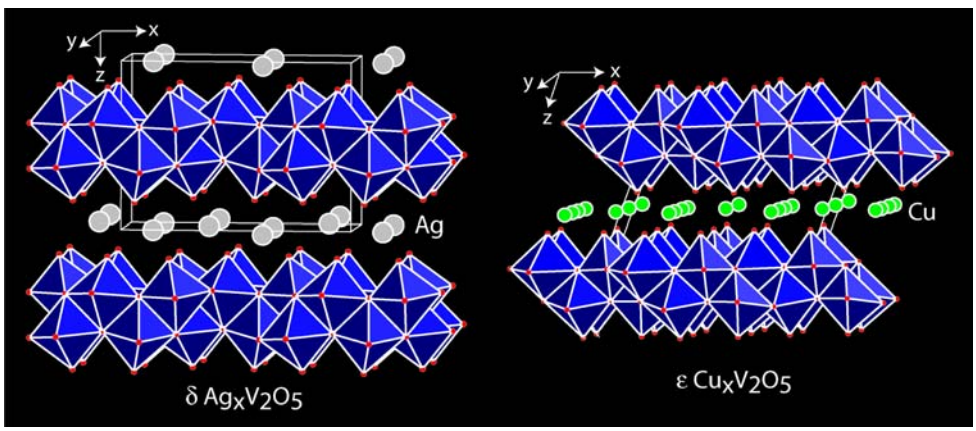

Fig. 5 View of the Cu and Ag intercalation between the $[V_2O_5]_n$ double layers in ε and δ $M_xV_2O_5$ bronzes

The final temperature and heating rate remained unchanged, i.e., 600 and 100 °C/min and pressure maintained during the whole experiment at 50 MPa. Here, three experiments with holding times of 0, 1 and 4 min at 600 °C are reported. It is worth pointing out the development of the blue $Cu_xV_2O_5$ phase to the detriment of V_2O_5 and correlatively, the decrease in copper slab with increasing holding times (Fig. 6). For each pellet, the same weighed amounts of V_2O_5 and Cu powders were placed in the carbon die.

The XRD pattern of the cross section with linear beam parallel to the axis of the cylindrical pellet is given in Fig. 7.

The ε $Cu_xV_2O_5$ has been clearly identified in spite of the strong orientation of the crystallites along the [010] crystallographic direction which is a common feature of the V_2O_5 and $M_xV_2O_5$ phases related to the short *b* axis (3.6–3.8 Å). If the ε phase is present together with Cu metal, traces of β' or even α cannot be avoided. The cell data obtained after PXRD indexing, i.e., monoclinic system, space group *Cm*, $a = 11.747$ Å, $b = 3.674$ Å, $c = 8.947$ Å, $\beta = 111.6°$, are in good agreement with those determined on ε $Cu_xV_2O_5$ single crystal [15].

It is worth noting a marked orientation of the crystallites during the formation of the $Cu_xV_2O_5$ phase along the [010]

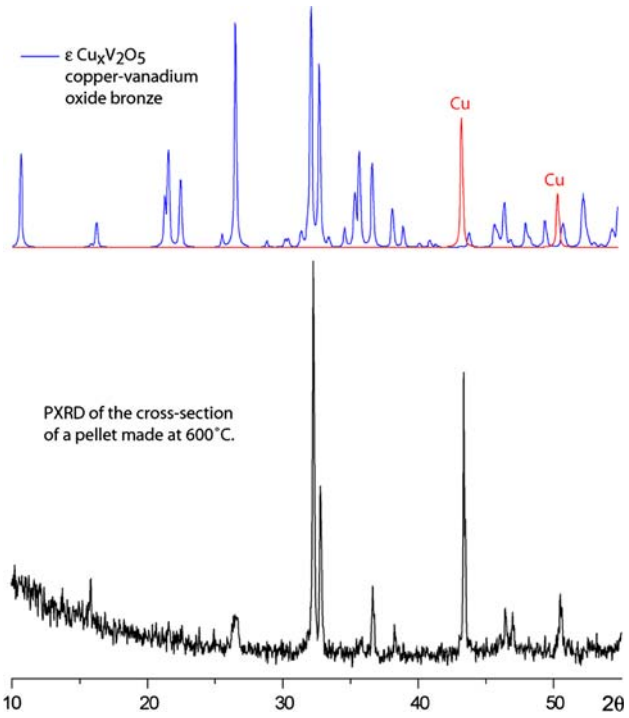

Fig. 7 PXRD of the pellet cross section (4 min)

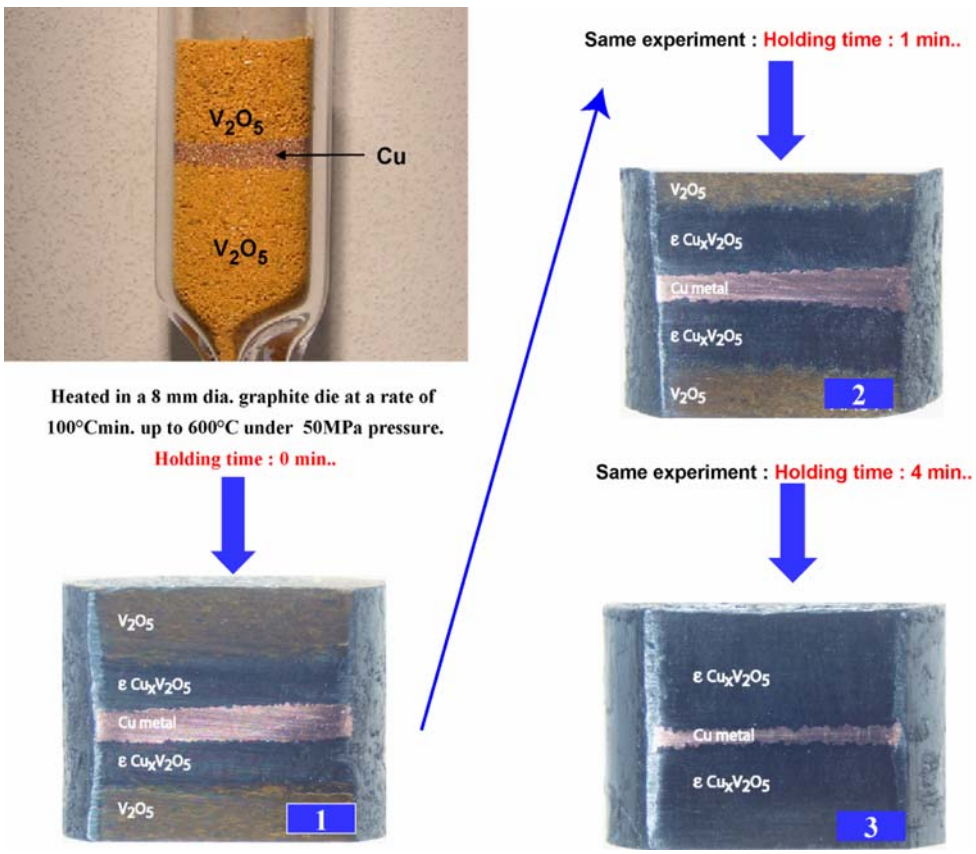

Fig. 6 Cross sections of pellets obtained after 0, 1 and 4 min holding times

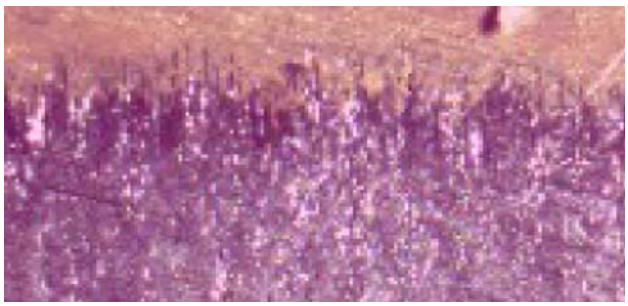

Fig. 8 Photo of the $Cu_xV_2O_5$ dendrites into V_2O_5

direction. This accounts for the quasi extinction of numerous *hkl* reflections. Looking at the border between the blue ε phase and the yellow V_2O_5 oxide, dendrites of the former phase growing in the latter phase are clearly evidenced (Fig. 8).

This assertion is demonstrated by PXRD on a series of pellet sections perpendicular to its axis starting from dendrites in V_2O_5 up to the one close to copper (sections T1–T4) (Fig. 9). The PXRD of the T1 pellet slice, in way of the dendrites, exhibits a significant peak enhancement around $2\theta = 50°$, while the pattern mainly reveals the presence of V_2O_5. Just after this peak, the 020 reflection corresponding to a $d_{020} = 1.781$ Å value which yields a b parameter of 3.562 Å is typical of V_2O_5 ($b = 3.564$ Å single crystal value [16]. The high peak corresponds to a reflection of the X-rays on the "summit" of the blue dendrites, the d_{020} value giving a b parameter, 3.626 Å, close to those of vanadium bronzes; its highest value is due to the presence of V^{4+}, a cation bigger than V^{5+}. The PXRD pattern on T2, with a slice 1 mm below T1, shows a slight displacement of the 020 dendrite reflection towards smaller 2θ angles giving $b = 3.685$ Å a value close to ε parameter (3.691 Å). Another peak appears; it belongs to ε phase, the V_2O_5 network is totally broken. A similar pattern can be noticed on the T3 pattern at a distance of 1 mm. T4 shows a more complete X-ray pattern clearly identified as that of the ε $Cu_xV_2O_5$ bronze, the surface of this slice being 0.3 mm away from the pure copper surface. PXRD patterns exhibit a small number of peaks that could be accounted for by the fact that Cu atoms behave like cannonballs hitting the V_2O_5 powder compact at very high speed and leaving no time for microcrystals network to get reorganized. The networks thus formed suffer some topological distortion and then behave as amorphous matter.

Cu and V concentrations have been investigated by electron microprobe technique using cross sections of the pellets like the former one shown in Fig. 3. Note that copper diffusion in all experiments is quasi-symmetrical apart from the slab of pure copper. In spite of the short reactive time, the copper concentration ratios (and vice versa the vanadium decrease) behave in the same manner as the pure Cu slab on both sides and seem little affected by direct current pulses.

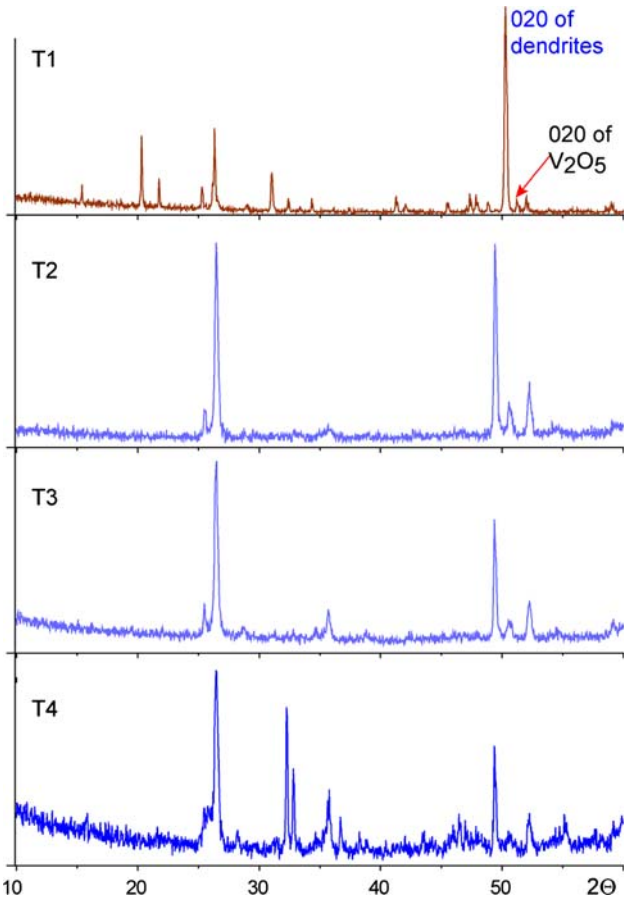

Fig. 9 PXRD patterns on the surface of T1, T2, and T4 sections of the pellet

Ag–V_2O_5 case

Similar experiments were conducted using silver powder. The temperature was slightly lowered to 550 °C but raised at the same rate of 100 °C/min, the maximum pressure being kept at 50 MPa. The same phenomenon occurs, with the formation of a blue phase, the δ $Ag_xV_2O_5$, whose structure is given in Fig. 5 [19]. In Fig. 10, the various parameters of one experiment corresponding to a holding time of 2 min at 550 °C are given. As can be seen on the figure pressure is stabilized at 50 MPa within 3 min. The beginning of sintering of powders takes approximately 4 min, it occurs around 360–380 °C, and is achieved in 2 min. Holding time does not bring about any improvement of the compaction.

A section of the pellet perpendicular to the die axis, right in the blue phase, was realized and a subsequent XRPD registered (Fig. 11). No trace of Ag metal or other α or β

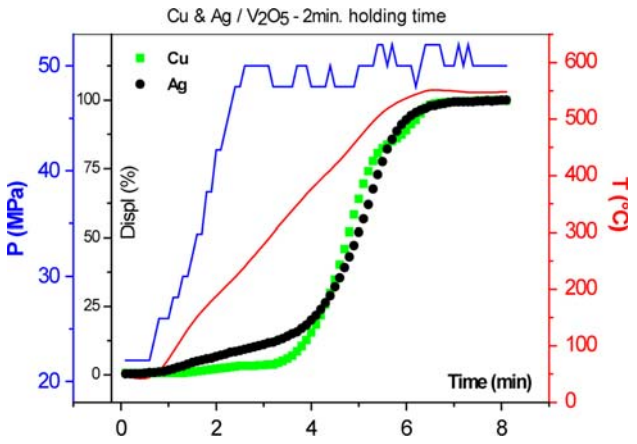

Fig. 10 Details of the SPS experiments (temperature, pressure, and relative compaction) of Cu and Ag atom interactions with V_2O_5

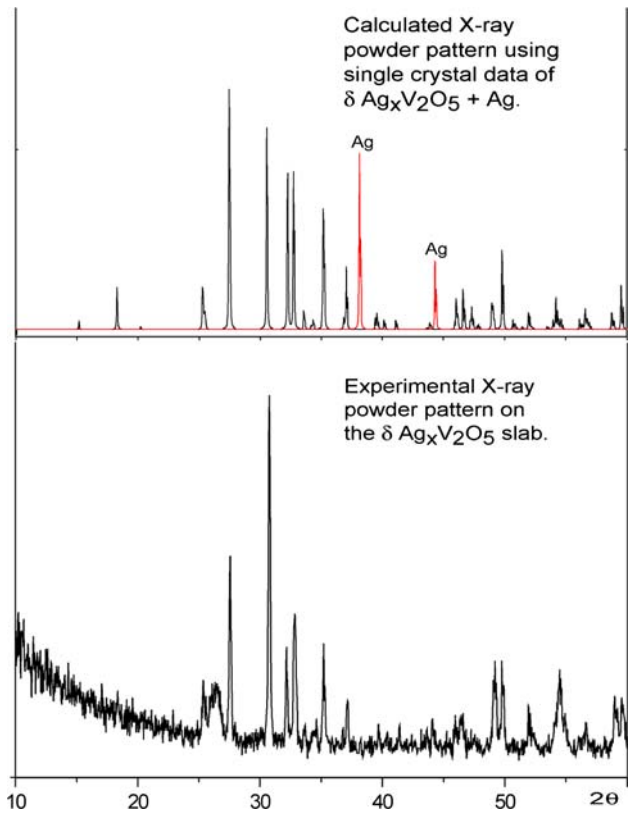

Fig. 11 Calculated and experimental XRPD of δ $Ag_xV_2O_5$

phases was found. The cell parameters derived from CELREF refinement of this powder pattern and based on monoclinic system—space group *C2/m*, are: $a = 11.699$ Å, $b = 3.659$ Å, $c = 8.731$ Å, $\beta = 90.57$. They are in good agreement with the ones determined from a single crystal study [19]. As in the Cu case major crystallite orientation effects accounting for the intensity variation of the *hkl* reflections can be noticed. The experimental XRP pattern shows that the silver bronze phase is free of silver metal.

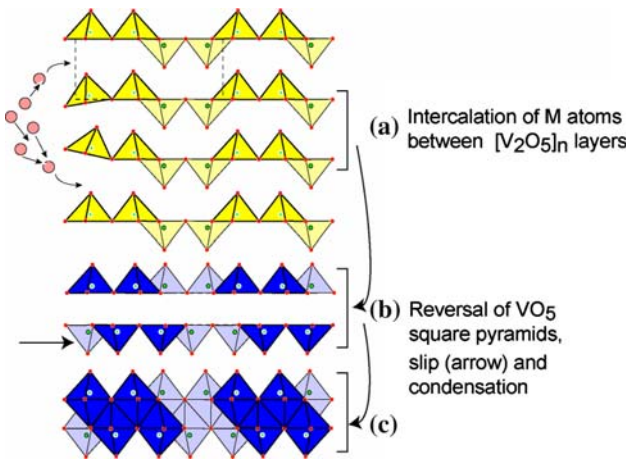

Fig. 12 Proposed mechanism for the formation of $[V_2O_5]_n$ double layers of the ε or δ phases

Structural mechanism for ε or δ formation

Structural mechanisms have been described elsewhere for several structures derived from V_2O_5 [22]. In the present case, the mechanism could be the result of the insertion of M atoms between every two successive $[V_2O_5]_n$ single layers slightly closing the interlayer and generating rotation of VO_5 square pyramids. Then, a slip parallel to the layers, indicated by the arrow, is followed by a collapse of the single layers to build up the double layers typical of the ε and δ $M_xV_2O_5$ bronze (top and bottom in upper part of Fig. 12). This mechanism does not rule out the possibility of getting some particles with the α or β $M_xV_2O_5$ structures. The formation of β' or β phases which corresponds to a more complex mechanism, may be due to the fact that they occur in small amounts and are not detected by XRPD. However they are clearly evidenced by scanning electron microscopy.

Atomic diffusion in V_2O_5

To account for the fast formation kinetics of the $Cu_xV_2O_5$ and $Ag_xV_2O_5$ phases, Cu and Ag diffusion mechanisms have been examined. Study of diffusion of Cu has been reported in a previous paper [23], and Ag diffusion follows the same experimental procedure. Recall here the results obtained for Cu diffusion and compare them with Ag diffusion.

Diffusion coefficients have been calculated according to Crank [24] from concentration profiles obtained by EDX and EPMA line-scans as shown in Fig. 13. Remarkably high values are obtained especially for Cu in ε $Cu_xV_2O_5$ (see Fig. 13, left) whose diffusion coefficient is of the same order of magnitude as self-diffusion in liquid metals. This high value is due to the large space used by Cu atoms

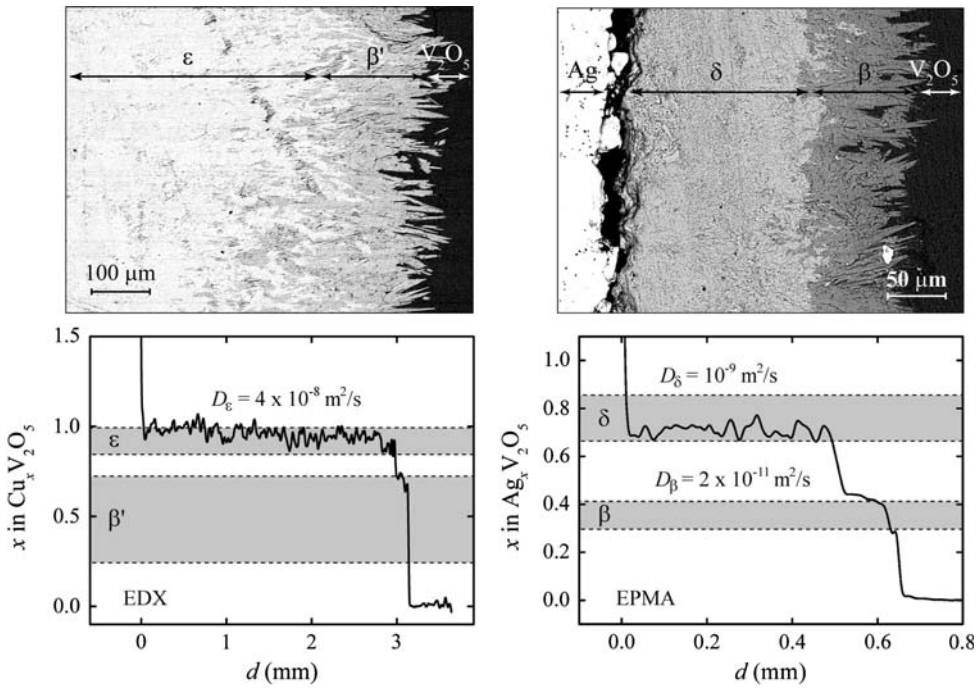

Fig. 13 (*Left, up*) BSE image of the extremity of the $Cu_xV_2O_5$ phase that has extended from the pure Cu source to the left (not shown in the figure). The zones corresponding to the ε and β' phases are indicated. (*Left, bottom*) EDX line-scan across the $Cu_xV_2O_5$ phase. The small plateau at $d \approx 3$ mm corresponds to the extension of the β' phase (experimental conditions: 500° C, 16 min, for BSE image and line-scan). (*Right, up*) BSE image of the $Ag_xV_2O_5$ phase that has extended from the pure Ag source to the left. The zones corresponding to the δ and β phases are indicated. (*Right, bottom*) EPMA line-scan across the $Ag_xV_2O_5$ phase (experimental conditions: 500° C, 8 min). On the line-scans, the domains of the phases are indicated as shaded areas, as well as the values of the diffusion coefficients in these phases

available to diffuse between the double $[V_2O_5]$ layers. In the Ag–V_2O_5 system, the diffusion coefficient in β phase is lower than in δ phase. The same is qualitatively observed in the Cu–V_2O_5 system, though the diffusion coefficient in β' phase cannot be determined due to the exceedingly small extension of this phase.

We interpret these differences in diffusion coefficient values as arising from the diffusion mechanisms that can reasonably be inferred from the (β', β) and (ε, δ) structures: the atomic jumps can take place either in one dimension along tunnels in the former, or in two dimensions between the double $[V_2O_5]$ layers in the latter. However, even if diffusion mechanisms are similar in the concentrated (ε and δ) structures, due to crystallographic similarities, their kinetics differ: Cu diffuses faster than Ag. Thus $D \approx 4 \times 10^{-8}$ m²/s in ε $Cu_xV_2O_5$ [18] and $D \approx 0.5$–1×10^{-9} m²/s in δ $Ag_xV_2O_5$ (in this study). This can be accounted for by comparing the space available to Cu and Ag atoms in the structure, given by the ratio between the spacing d of the $[V_2O_5]$ layers in each structure ($Cu_xV_2O_5$ and $Ag_xV_2O_5$) and the ionic radius r of the diffusing atom. With values d of 2.32 and 3.03 Å for $Cu_xV_2O_5$ and $Ag_xV_2O_5$, respectively, and values r of 0.5–0.6 Å and 1–1.1 Å for Cu and Ag, respectively, we get $d/r = 3.9$–4.6 for $Cu_xV_2O_5$ and 2.8–3 for $Ag_xV_2O_5$. Then, if it is assumed that the mobility of diffusing atoms is greatly affected by steric considerations, it is not surprising that Cu is more mobile than Ag in V_2O_5. The fact that copper atoms can occur under their two oxidation states, 1+ and 2+, may also explain the difficulty in creating a well-defined crystallographic site, as demonstrated in β' $Cu_xV_2O_5$ and $Cu_{2.33-x}V_4O_{11}$ crystal structures [17, 25] while it is not the case for Ag atoms. This could account for the high mobility of copper in the V_2O_5 network.

Kinetics cannot be compared in the less concentrated phases (β, β') because experimental data become too inaccurate.

Finally, D values are higher by eight orders of magnitude than those obtained by a galvanostatic pulse technique described in [26]. This discrepancy is difficult to explain, even if the possible involvement of SPS current pulses in the diffusion acceleration is considered. Diffusion enhancement by high current densities is known as electromigration. This effect has been proposed as a key factor in the SPS synthesis for conducting materials [6]. However, V_2O_5, in which Ag diffuses, is very poorly conducting; and one must also consider that as soon as the bronze phase is formed the powder becomes semiconductor with an energy gap around 0.3–0.5 eV due to the electron hopping phenomenon between V^{4+} and V^{5+}. Hence, the current density

should be low in the sample at the beginning of the synthesis with an increase as soon as the bronze phases are formed. Consequently, electro-migration should play only a minor role in the Ag diffusion processes. To overcome all these difficulties, we intend to conduct impedance spectroscopy experiments on δ $Ag_xV_2O_5$ samples compacted by SPS and by conventional compaction techniques, and to compare the results.

Cu–V_2O_5–Ag case

Following these experiments, it was tempting to assess the behaviour of both Cu and Ag systems during SPS syntheses. The question was that of knowing what happens when these $Cu_xV_2O_5$ and $Ag_xV_2O_5$ phases under formation by SPS process come into contact? To address this issue a slab of V_2O_5 powder sandwiched by Cu and Ag powders was placed in the graphite die as schematized in Fig. 14a. The SPS process was as follows: maximum temperature 520 °C, raised at a rate of 100 °C/min, pressure fixed at 75 MPa, holding time being 8 min. The study of the pellet by SBE of the cross section reveals a surprising phenomenon.

As expected, the domain of the Cu phases is a lot more extended and homogeneous than the Ag one. This last domain of the $Ag_xV_2O_5$ phases appears extremely perturbed with major white traces (Fig. 14b). In Fig. 14b, the important part of pure $Cu_xV_2O_5$ phase has been omitted to focus on the Ag part. In the median part of the micrograph, the matrix previously made up of $Ag_xV_2O_5$ is now composed of a rich-Cu phase also containing some remaining diluted Ag islets becoming increasingly important the closer one gets to the silver source with large "deposits" of metallic Ag filaments.

As Cu and Ag diffuse in V_2O_5, the $Cu_xV_2O_5$ and $Ag_xV_2O_5$ phases extend towards each other, then contact and inter-react. Figure 15 shows the inter-reaction region. Originating from the left, Cu has diffused throughout the sample up to the metallic Ag to the right, as shown by EDS line-scan analyzes (Fig. 15). White filaments, identified as metallic Ag by EDS point analyses, are seen in lieu of $Ag_xV_2O_5$. Between the Ag filaments, the matrix, formerly rich in Ag, is now rich in Cu. These findings evidence the fact that when Cu reaches $Ag_xV_2O_5$, some Ag atoms are removed from the matrix and coalesce in the form of metallic precipitates. This probably results from the size difference between the Cu and Ag atoms. As Ag is bigger than Cu, it expands the distance between $[V_2O_5]_n$ layers. Then, Cu substitution for Ag would lead to relaxation of the structure and a decrease in free energy of this phase. However, we have first indications that the replacement of Ag by Cu in the V_2O_5 matrix is not complete, and that some Ag atoms remain "dissolved" in the Cu-containing structure. The matrix is then of the type $Cu_xAg_yV_2O_5$. We are now trying to determine the phase diagram of the $Cu_xAg_yV_2O_5$ system as well as the crystalline structure of a ternary phase as a function of Cu and Ag relative contents in V_2O_5 observed in solid state classical reactions.

Conclusion

Finally, note that these experiments provide an original flash syntheses of phases using the Spark Plasma technique for purposes other than sintering such as creating new networks. For example it is significant that the "bombing" of V_2O_5 network with atoms, here Cu, brings about phases by destroying and shearing the former network and rebuilding simultaneously a new one in a significant

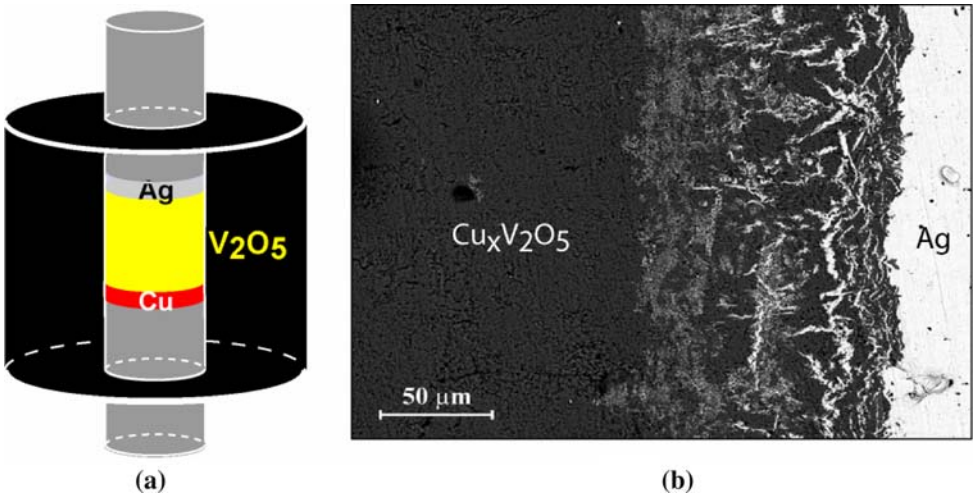

Fig. 14 (**a**) Schematic view of the graphite die containing successive layers of Cu, V_2O_5 and Ag powders. (**b**) BSE view of the $Cu_xV_2O_5$ and $Ag_xV_2O_5$ inter-reaction region

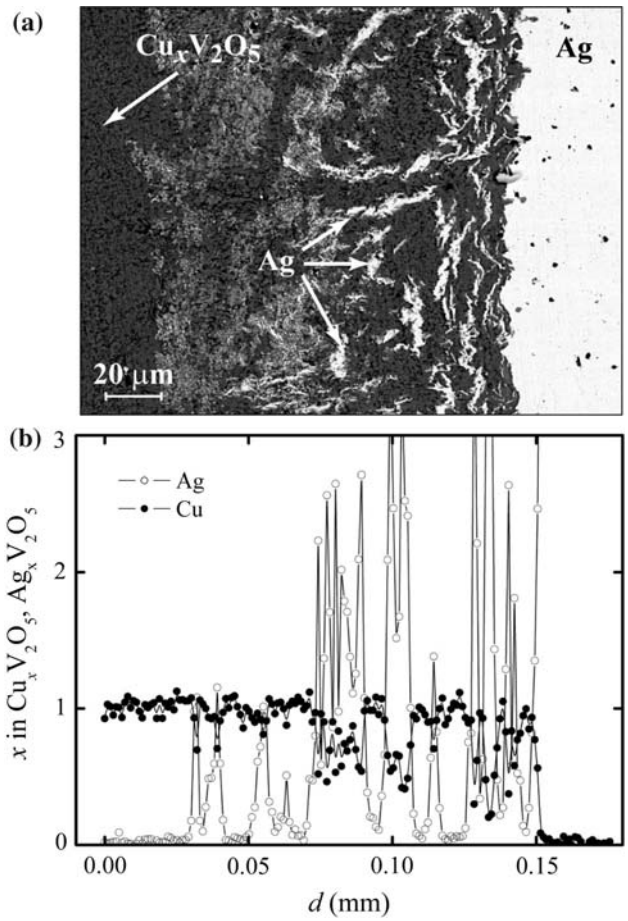

Fig. 15 (**a**) BSE micrograph of a selection of the cross section of the pellet in the perturbed $Ag_xV_2O_5$ region, for analysis of this matrix previously composed of $Ag_xV_2O_5$ and now of a rich-Cu phase also containing some remaining dissolved or intercalated Ag and metallic Ag filaments. (**b**) EDS line-scan along a horizontal line across the above BSE micrograph. Peaks in the Ag signal are due to the small metallic Ag filaments

quantity. Ag atoms do the same even if it occurs in a smaller volume. The Cu ability to extract Ag atoms from δ $Ag_xV_2O_5$ phase to form Ag islet or filaments was unexpected and paves the way for new investigations about this phenomenon. This can also be compared with the insertion–extrusion of Cu with the formation of dendrites in the $Cu_{2.33-x}V_4O_{11}$ phase [18] and to the extension of this Cu power against other silver phases or any other ones. Note that these $M_xV_2O_5$ phases, have required careful grinding of the corresponding powders and long treatments, i.e., 2 days, in sealed quartz tubes at 600 °C. An interesting route to develop new solid state chemistry in all the fields of oxides, fluorides, oxide-fluorides, nitrides … is fully open and will extend the possibilities to understand what happens at the interfaces of two different powders constituting a single pellet sintered by SPS.

Acknowledgement The Centre National de la Recherche Scientifique (France) is gratefully acknowledged for its financial support.

References

1. Tokita M (1999) Mater Sci Forum 83:308
2. Omori M (2000) Mater Sci Eng A 287:183. doi:10.1016/S0921-5093(00)00773-5
3. Shen ZJ, Johnsson M, Zhao Z, Nygren M (2002) J Am Ceram Soc 85(8):1921
4. Anselmi-Tamburini U, Genari S, Garay JE, Munir ZA (2005) Mater Sci Eng 394:139. doi:10.1016/j.msea.2004.11.019
5. Chen W, Anselmi-Tamburini U, Garay JE, Groza JR, Munir ZA (2005) Mater Sci Eng 394:132
6. Munir ZA, Anselmi-Tamburini U, Ohyanagi M (2006) J Mater Sci 41:763. doi:10.1007/s10853-006-6555-2
7. Locci AM, Orru R, Cao G, Sanna S, Congiu F, Concas G (2006) AICHE J 52(7):2618
8. Yamauchi A, Yoshimi K, Kurokawa K, Hanada S (2007) J Alloys Compd 434–435:420–3
9. Recknagel C, Reinfried N, Hohn P, Schnelle W, Rosner H, Grin Yu, Leithe-Jasper A (2007) Sci Technol Adv Mater Elsevier Science Ltd 8(5):357
10. Inagaki J, Sakai Y, Uekawa N, Kojima T, Kakegawa K (2007) Mater Res Bull 42(6):1019
11. Cao G, Locci AM, Orru R, Munir ZA (2006) Mater Sci Eng A Struct Mater Prop Microstr Process 434(1–2):23
12. Wadsley AD (1955) Acta Cryst 8:695
13. Wadsley AD (1957) Acta Cryst 10:261
14. Casalot A, Deschanvres A, Hagenmuller P, Raveau B (1965) Bull Soc Chim Fr XC 1730
15. Galy J, Lavaud D, Casalot A, Hagenmuller P (1970) J Solid State Chem 2:531
16. Lavaud D, Galy J (1971) Acta Cryst B27:1005
17. Savariault JM, Deramond E, Galy J (1994) Z für Kristallogr 209:405
18. Morcrette M, Rozier P, Dupont L, Mugnier E, Sannier L, Galy J, Tarascon J-M (2003) Nat Mater 2:755
19. Andersson S (1965) Acta Chem Scand 19:1371
20. Deramond E, Savariault JM, Galy J (1994) Acta Cryst C50:164
21. Enjalbert R, Galy J (1986) Acta Cryst C42:1467
22. Galy J (1992) J Solid State Chem 100:209
23. Monchoux JP, Galy J (2008) J Solid State Chem 181:693
24. Crank J (1956) The Mathematics of Diffusion. Clarendon Press, Oxford
25. Rozier P, Satto C, Galy J (2000) Solid State Sci 2(6):595
26. Sholtens BB (1976) Mat Res Bull 11:1533